Check for updates

Journal of Vinyl and Additive Technology

WILEY | spe INSPIRING PLASTICS PROFESSIONALS

RESEARCH ARTICLE

Investigation of Mechanical Properties in Layered Multi-Material 3D Printing Using Commercial Filaments: Direct Stacking of ABS, PA, and Compatibilizing Layers

Sinan Yilmaz[1] | Okan Gul[2] | Onur Coban[3]

[1]Department of Mechanical and Material Technologies, Kocaeli University, Kocaeli, Turkey | [2]Department of Mechanical Engineering, Faculty of Engineering, Kocaeli University, Kocaeli, Turkey | [3]Faculty of Aeronautics and Astronautics, Kocaeli University, Kocaeli, Turkey

Correspondence: Sinan Yilmaz (sinan.yilmaz@kocaeli.edu.tr)

Received: 25 July 2025 | **Revised:** 18 November 2025 | **Accepted:** 21 November 2025

Keywords: compatibilizing layers | fused filament fabrication (FFF) | interfacial bonding | mechanical characterization | multi-material 3D printing (MM3DP)

ABSTRACT

Fused filament fabrication (FFF) technology has rapidly progressed in software and equipment, driven by increasing demand across industries and households. However, the development of compatible and high-performance materials has lagged, limiting the mechanical integrity and design flexibility of printed components. To address this issue, this study investigates the interfacial bonding behavior of multi-material structures composed of acrylonitrile butadiene styrene (ABS) and polyamide (PA), two polymers that are chemically incompatible. To enhance interfacial adhesion, three commonly used thermoplastic filaments were employed as intermediate compatibilizing layers. Mechanical characterization was performed through tensile and interlaminar shear strength tests to evaluate bonding performance. All compatibilizing layers improved adhesion between ABS and PA, yielding up to 32% higher tensile strength and 43% higher interlaminar shear strength compared to direct stacking. Fractographic observations confirmed these results by revealing distinct failure patterns and improved interfacial continuity. Overall, the findings demonstrate a practical method for achieving strong adhesion between incompatible polymers without surface treatments or adhesives, offering guidance for the design of hybrid structures and expanding the potential of the technology.

1 | Introduction

Additive manufacturing (AM), a general term encompassing various fabrication processes, has the potential to rapidly transform modern production. Unlike conventional machining, which removes material through subtractive operations, AM builds parts layer by layer, enabling the direct fabrication of complex geometries from digital designs [1]. Among these methods, fused filament fabrication (FFF) stands out due to its simplicity, cost-effectiveness, and compact equipment requirements. These features make it accessible for both industrial and research applications [2]. The versatility of FFF in producing customized components has resulted in widespread adoption across sectors such as automotive, aerospace, healthcare, and consumer products [3, 4].

In recent years, FFF technology has advanced substantially in terms of hardware, software, and process control. However, despite these improvements, the mechanical strength of printed parts remains considerably lower than that of cast or molded components [5]. This limitation restricts the use of FFF in demanding engineering applications where high strength and reliability are required. The relatively low strength mainly results from the process nature, which leads to void formation

© 2025 Society of Plastics Engineers.

Highlights

- Compatibilizing layers improved interfacial bonding in dual material prints through direct stacking of commercial filaments.
- Tensile and ILSS tests confirmed mechanical improvements.
- PLA gave the highest increases in yield strength and ILSS.
- PETG showed the best overall performance considering all properties.
- TPU enhanced ILSS despite its lower intrinsic mechanical properties.

within the cross-section and incomplete fusion between adjacent strands. To mitigate these defects, parameters such as nozzle and bed temperatures, printing speed, infill rate, and layer orientation are optimized. Nevertheless, numerous studies have shown that, among all process-related factors, the material type plays the most decisive role in determining the mechanical performance of FFF parts [6].

Various thermoplastic materials commonly used in FFF, including acrylonitrile butadiene styrene (ABS), polyamide (PA), polylactic acid (PLA), thermoplastic polyurethane (TPU), and polyethylene terephthalate glycol (PETG). Each provides distinct mechanical, thermal, and chemical characteristics suitable for specific applications [7, 8]. For instance, PA offers high toughness and wear resistance, whereas ABS provides excellent dimensional stability and surface finish [9–11]. PLA and PETG are known for their ease of printing and dimensional accuracy, whereas TPU is valued for its flexibility and impact resistance. Despite these individual advantages, single-material printed parts often fail to meet the combined demands of strength, durability, and functionality required in engineering applications. This limitation has encouraged researchers to explore multi-material 3D printing (MM3DP) as an effective approach to combine complementary properties within a single component [12–15].

Multi-material 3D printing (MM3DP) enables the fabrication of parts that integrate polymers with complementary properties, offering design flexibility and localized control of mechanical or thermal performance [13–15]. The approach allows functional gradients, improved material efficiency, and weight reduction through selective material placement. These advantages make MM3DP an attractive method for creating components with tailored performance. For example, in gear manufacturing, the teeth can be printed using PA to exploit its toughness and wear resistance, whereas the gear body can be made from ABS to take advantage of its dimensional stability and surface quality. This strategy enhances overall performance, reduces weight and cost, and allows localized control of thermal and mechanical behavior [16–18]. However, the process also presents several challenges. Differences in chemical composition and thermal behavior between dissimilar materials can lead to weak interfacial bonding, void formation, and dimensional inaccuracy. Such issues increase porosity and surface roughness, reducing the overall strength, hardness, and structural integrity of the printed part [19]. In layered or sandwich-structured components, the type and compatibility of the materials are therefore the dominant factors influencing mechanical response. Compatibility depends on the similarity of the polymers' chemical structure, thermal characteristics (expansion and shrinkage), and physical properties such as viscosity and surface texture.

Previous studies have explored strategies to improve interfacial bonding in multi-material polymer systems via chemical or process-based interventions. Post-processing annealing (thermal treatments) has been used to promote polymer chain mobility and inter diffusion across interfaces, thereby enhancing adhesion; however, in dissimilar polymers with different transition temperatures, annealing may introduce residual stresses, warping, or degrade mechanical integrity (e.g., "Effects of functionalization and annealing in enhancing the interfacial bonding" study) [20]. Surface activation techniques such as plasma or corona treatment can increase surface energy and introduce polar groups to facilitate bonding, but their effects often remain superficial and diminish over time due to surface rearrangement or aging (discussed in reviews of interlayer bonding in fused deposition methods) [21, 22]. Hybridization approaches (e.g., the use of compatibilizer interlayers or functionalized coatings between dissimilar polymers) have shown promise (e.g., combining styrene maleic anhydride compatibilizer into ABS/PA blends) but often suffer from challenges in process integration, non-uniform interlayer thicknesses, or limited reproducibility within 3D printing environments [23]. Given these trade-offs and gaps, a systematic investigation of compatibilizing interlayers specifically in the MM3DP context is warranted.

In most reported MM3DP studies, researchers have preferred chemically compatible polymer pairs such as PLA/ABS or ABS/PETG to ensure sufficient interfacial adhesion [24–26]. Although these combinations simplify processing, they also limit the range of achievable material properties. In this study, two chemically incompatible polymers, acrylonitrile butadiene styrene (ABS) and polyamide (PA), were selected to investigate their interfacial bonding behavior in layered multi-material printing. The incompatibility between these materials arises from their distinct chemical and thermal characteristics: PA is semi-crystalline with a glass transition temperature (T_g) of about 55°C, whereas ABS is amorphous with a T_g around 105°C. These differences hinder molecular diffusion across the interface and reduce interlayer adhesion. However, they also present an opportunity to combine the toughness and wear resistance of PA with the dimensional stability and surface quality of ABS in a single structure [27–31].

Since ABS and PA are chemically incompatible, achieving strong interfacial bonding between them requires an intermediate compatibilizing layer. In this study, three commonly used commercial filaments (PLA, PETG, and TPU) were selected as potential compatibilizers to enhance adhesion between ABS and PA layers. This approach provides a practical route for improving interfacial bonding without the need for additional surface treatments, chemical modification, or custom material synthesis. By utilizing readily available filaments, the

15480585, 0, Downloaded from https://4spepublications.onlinelibrary.wiley.com/doi/10.1002/vnl.70051 by Sinan YILMAZ - Kocaeli Universitesi , Wiley Online Library on [06/12/2025]. See the Terms and Conditions (https://onlinelibrary.wiley.com/terms-and-conditions) on Wiley Online Library for rules of use; OA articles are governed by the applicable Creative Commons License

method offers an easily applicable and scalable strategy that can be directly implemented in standard FFF systems.

To date, no systematic study has been reported on the interfacial adhesion between directly stacked ABS and PA layers fabricated by FFF. The objective of this work is to examine the bonding behavior of these incompatible polymers, assess the influence of intermediate compatibilizing layers, and provide insights for interface design, material selection, and process optimization in multi-material 3D printing. The findings of this study are expected to provide new insights into the interfacial mechanics of chemically incompatible thermoplastics in MM3DP, offering a quantitative understanding of how compatibilizer selection influences adhesion and mechanical performance.

2 | Materials and Methods

This section outlines the materials and 3D printing parameters used to fabricate the test specimens, followed by the detailed description of the sample configurations. It also presents the characterization methods and testing conditions employed to evaluate the structural and mechanical performance of the printed parts.

2.1 | Filaments and 3D Printing Process

In this study, five different commercial filaments produced by ESUN were used: ABS+ (black), PA (transparent), PLA+ (black), PETG (white), and TPU 95A (black), all with a diameter of 1.75 mm. The specimens were fabricated using a Creality K1 Max 3D printer. Slicing was performed using Creality Print software (version 5.0). Prior to printing, all filaments were dried in a vacuum oven at 45°C for 12 h. The material properties provided by the manufacturers are summarized in Table 1, and the 3D printing parameters are listed in Table 2. A schematic representation of the 3D printing setup and specimen orientation is shown in Figure 1, whereas Figure 2 presents optical microscope images of the MM3DP specimens. In the layered 3D printing of ABS and PA, samples were fabricated with an alternating layer configuration in a 1:1 ratio. Since the thicknesses of the tensile and ILSS specimens differ (2 mm for tensile and 4 mm for ILSS), the reference ABS/PA samples were printed with 5 and 10 alternating layers of 0.2 mm thickness, respectively. Since

TABLE 1 | Overview of key properties of the filament materials based on material safety data sheets available on the ESUN brand's website at the time when the materials were provided.

Property	Unit	ABS+	PA	PLA+	PETG	TPU 95A
CAS number		9003-56-9	32131-17-2	26100-51-6	25038-59-9	502-44-3
Additives	wt%	1	1	4–8	5	—
Density	g/cm[d]	1.06	1.12	1.24	1.27	1.21
Heat dist. temp.	°C, 0.45 MPa	73	50	53	—	—
Melt flow index		15[b]	5[c]	5[d]	20[d]	1.2[d]
Tensile strength[a]	MPa	40	57	53	52	35
Elongation at break[a]	%	30	196	4	83	800
Flexural strength[a]	MPa	68	57	81	58	—
Flexural modulus[a]	MPa	2443	1495	2888	1073	—
IZOD impact strength[a]	kJ/m[c]	42	15	6	5	—
Print temperature	°C	220–260	230–260	210–230	203–250	220–250
Bed temperature	°C	90–110	80–90	45–60	75–90	45–60

[a]X-Y print orientation.
[b]220°C/10 kg.
[c]230°C/2.16 kg.
[d]190°C/2.16 kg.

TABLE 2 | Experimental parameters for 3D printing.

Layer height (mm)	Wall line count	Pattern	Infill density (%)	Orientation	Nozzle temperature (°C)[a]	Build plate	Build plate temperature (°C)[b]	Speed (mm/s)
0.2	2	Lines	100	XYZ	230	Smooth PEI	90	100

[a]All samples were fabricated using a 0.4 mm brass nozzle.
[b]Applicable only for MM3DP specimens; for single-material samples, the bed temperatures given in Table 1 were used.

15480585, 0, Downloaded from https://4spepublications.onlinelibrary.wiley.com/doi/10.1002/vnl.70051 by Sinan YILMAZ - Kocaeli Universitesi , Wiley Online Library on [06/12/2025]. See the Terms and Conditions (https://onlinelibrary.wiley.com/terms-and-conditions) on Wiley Online Library for rules of use; OA articles are governed by the applicable Creative Commons License

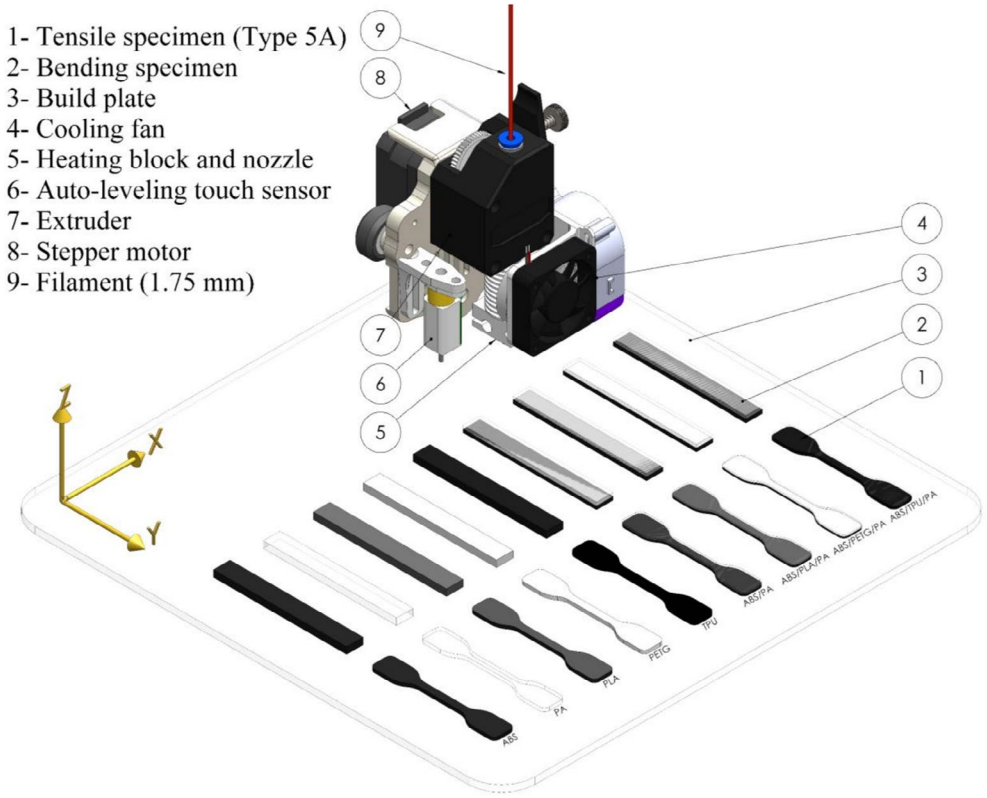

FIGURE 1 | Schematic illustration of the 3D printing setup and specimen orientation.

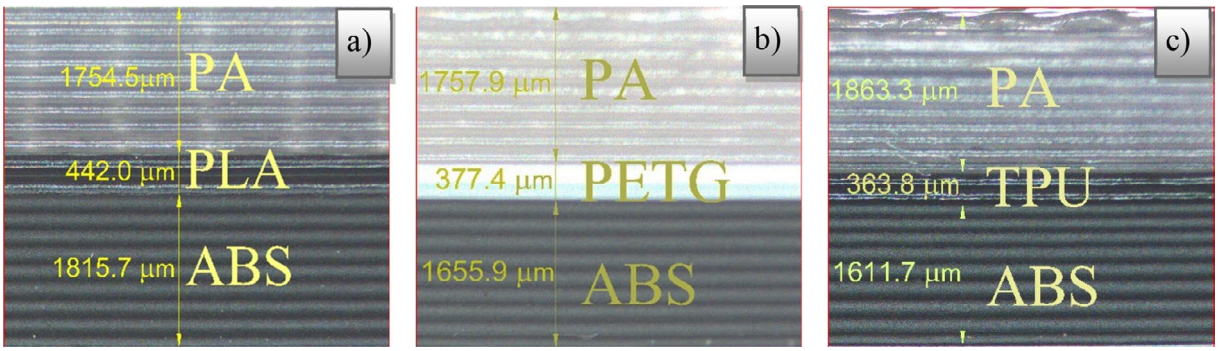

FIGURE 2 | Representative cross-sectional views of additively manufactured laminar composite structures: (a) ABS_PLA_PA, (b) ABS_PETG_PA and (c) ABS_TPU_PA.

TABLE 3 | Tensile test results of all specimens.

Material	Ultimate tensile strength (MPa)	Tensile modulus (MPa)	Tensile strain (%)
ABS	36.6 ± 0.8	2013.5 ± 19.1	4.2 ± 0.4
PA	48.2 ± 0.1	767.5 ± 30.4	141.4 ± 0.5
PLA	51.6 ± 1.7	2867.0 ± 48.1	8.8 ± 0.5
PETG	45.1 ± 0.3	1802.0 ± 26.9	76.5 ± 22.0
TPU	20.9 ± 0.1	55.0 ± 0.1	299.7 ± 0.4
ABS_PA	24.7 ± 0.9	1379.5 ± 4.9	119.6 ± 17.6
ABS_PLA_PA	32.7 ± 0.1	1699.0 ± 39.6	10.2 ± 1.8
ABS_PETG_PA	31.8 ± 0.5	1464.5 ± 77.1	422.6 ± 32.0
ABS_TPU_PA	25.9 ± 1.0	1094.5 ± 0.7	285.3 ± 0.4

15480585, 0, Downloaded from https://4spepublications.onlinelibrary.wiley.com/doi/10.1002/vnl.70051 by Sinan YILMAZ - Kocaeli Üniversitesi , Wiley Online Library on [06/12/2025]. See the Terms and Conditions (https://onlinelibrary.wiley.com/terms-and-conditions) on Wiley Online Library for rules of use; OA articles are governed by the applicable Creative Commons License

there was no interfacial adhesion in the ABS/PA samples (as the layers remained separated), optical microscope images could not be taken. Therefore, only the optical microscope images of the MM3DP samples containing compatibilizing layers were included in Figure 2.

The specimen configurations shown in Figure 2 were designed to examine the effect of intermediate compatibilizing layers (PLA, PETG, and TPU) on interfacial bonding between two chemically incompatible polymers, ABS and PA. The optical microscope images presented in Figure 2 illustrate the layer arrangement and verify the structural integrity and dimensional stability of the multilayer 3D printed specimens. The absence of warping was determined through visual inspection, based on the parallel and horizontally aligned strand geometry, indicating that the inserted intermediate layers effectively minimized thermal distortion. A uniform bed temperature of 90°C was used for all multi-material prints, since ABS was always deposited first and requires a higher bed temperature to maintain adhesion and reduce distortion. The specimens consist of nine (9) layers of either ABS or PA, with two intermediate layers of either PLA, PETG, or TPU positioned between them, maintaining equal numbers of ABS and PA layers on both sides. The nominal total thickness of the specimens was designed as 4 mm with a 0.2 mm layer height; however, the measured total thickness varied between approximately 3.8 mm and 4.0 mm across different material combinations. These minor deviations are attributed to material-specific cooling behavior, thermal contraction, and slight process variations during printing. The printing process always starts with ABS as the first layer because ABS adheres better to the print bed, which is critical in 3D printing to prevent print failure. After the ABS layers, the intermediate material layers (if any) were printed, followed by the PA layers, ensuring stable adhesion and successful multilayer fabrication.

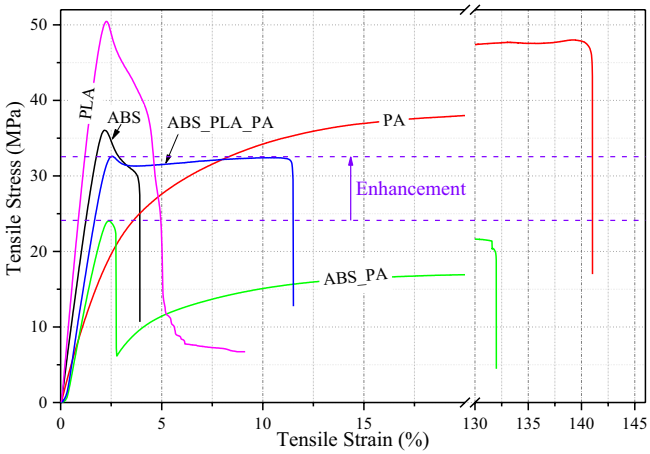

FIGURE 3 | Representative stress–strain curves of specimens: ABS, PA, PLA, ABS_PA, and ABS_PLA_PA.

2.2 | Material Characterization

2.2.1 | Tensile Test

Uniaxial tensile tests were conducted at room temperature using an Instron 4411 testing machine, applying a constant displacement rate of 2 mm/min. Type 5A specimens, prepared according to ISO 527 standard, were used for all tests. For each material

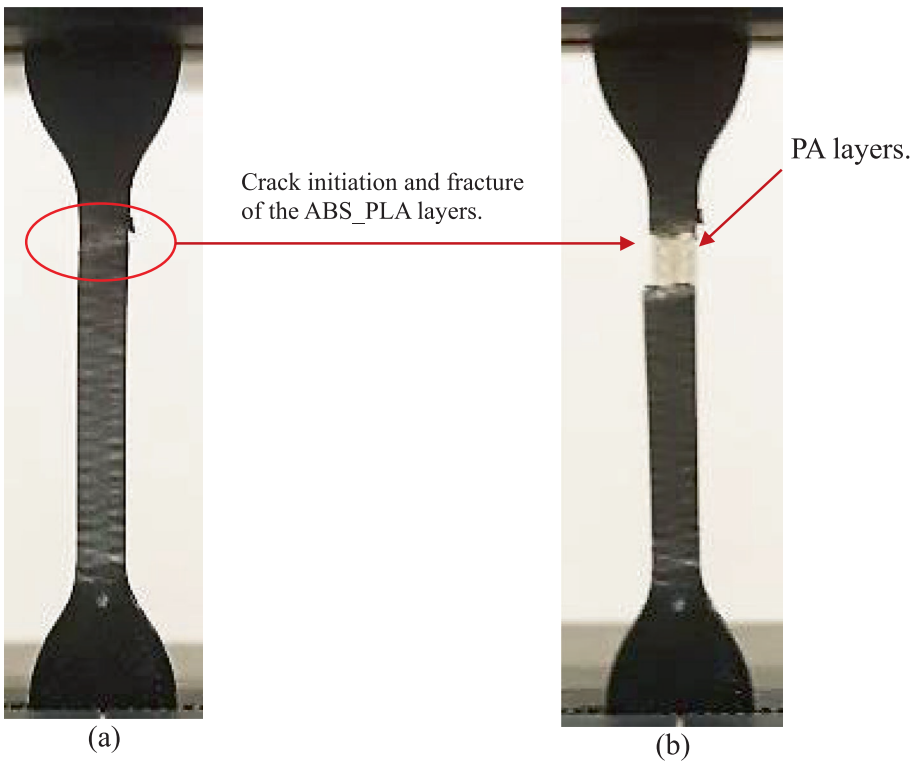

FIGURE 4 | Representative images of yield and fracture points of ABS_PLA_PA specimen: (a) ABS and PLA yielding together, (b) simultaneous fracture of ABS and PLA.

15480585, 0, Downloaded from https://4spepublications.onlinelibrary.wiley.com/doi/10.1002/vnl.70051 by Sinan YILMAZ - Kocaeli Üniversitesi , Wiley Online Library on [06/12/2025]. See the Terms and Conditions (https://onlinelibrary.wiley.com/terms-and-conditions) on Wiley Online Library for rules of use; OA articles are governed by the applicable Creative Commons License

combination, three specimens were tested, and average yield strength, elastic modulus, and elongation at break values were calculated.

2.2.2 | ILSS Test

The Instron 4411 testing machine was equipped with a three-point bending fixture in accordance with ASTMD2344 standards. Tests were conducted at room temperature with a crosshead speed of 2 mm/min. For each material combination, three samples were tested, and the recorded data were used to calculate average values of interlaminar shear strength. These calculations were performed using standard formulas [32, 33].

ILSS was calculated using the following formula derived from the three-point bending test [34]:

$$\mathrm{ILSS} = 0.75\frac{F_{\max}}{b.d}\ (\mathrm{MPa}) \tag{1}$$

where $F_{\max}$ represents the peak load (N), b is the specimen width (mm), and d is the specimen thickness (mm).

In these tests, specimens with dimensions of $10\times50\times4\,\mathrm{mm}^3$ were used, and a support span of 28 mm was selected. Although the standards recommend a span-to-thickness ratio of 4:1 to promote interlaminar shear failure, a span-to-thickness ratio of 7:1 was adopted due to constraints associated with the testing fixture, particularly the width of the loading nose, which required a larger span to prevent interference with the specimen [35]. The use of a 7:1 span ratio may introduce partial bending effects, and this is acknowledged as a methodological limitation. Since the primary objective of this study was to compare the interfacial performance of the different material combinations, a slight deviation from the recommended ratio was considered acceptable. During these tests, ABS layers were consistently positioned on the tensile side of the bending setup due to their relatively brittle nature, ensuring consistent crack initiation conditions and facilitating a more reliable comparison of interfacial performance across the specimens.

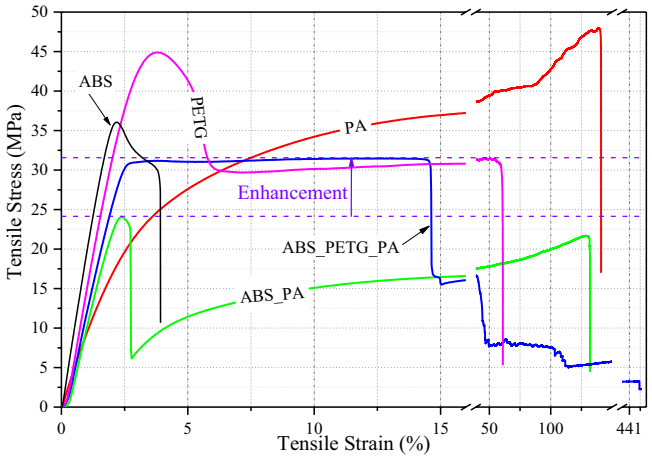

FIGURE 5 | Representative stress–strain curves of specimens: ABS, PA, PETG, ABS_PA, and ABS_PETG_PA.

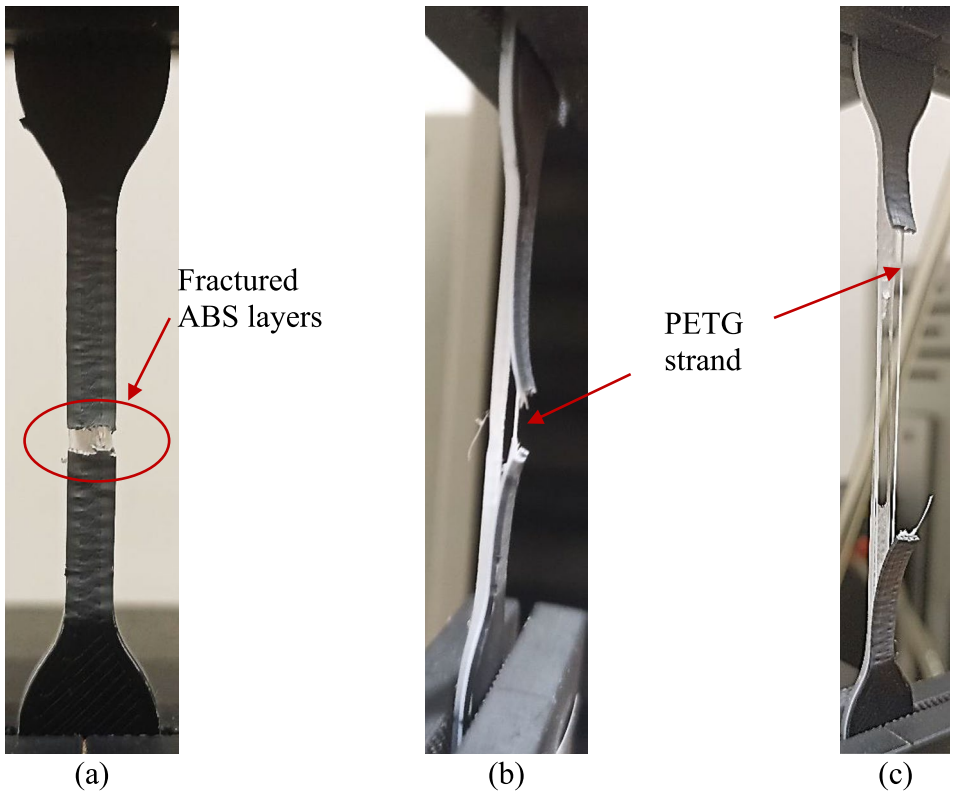

FIGURE 6 | Representative images showing yield and fracture points: (a) fracture of ABS, (b) fracture of PETG after simultaneous yielding of PETG and PA, and (c) yielding of PA and PETG wall lines prior to fracture.

15480585, 0, Downloaded from https://4spepublications.onlinelibrary.wiley.com/doi/10.1002/vnl.70051 by Sinan YILMAZ - Kocaeli Üniversitesi , Wiley Online Library on [06/12/2025]. See the Terms and Conditions (https://onlinelibrary.wiley.com/terms-and-conditions) on Wiley Online Library for rules of use; OA articles are governed by the applicable Creative Commons License

3 | Results and Discussion

This section presents the experimental results obtained from the fabricated specimens, including optical observations and mechanical test data. The results are discussed in relation to interfacial bonding quality, material compatibility, and the effectiveness of the intermediate layers. Each subsection follows the sequence of visual analysis, tensile performance, and interlaminar shear strength to highlight the correlations between structural integrity and mechanical behavior.

3.1 | Tensile Test Results

The tensile test results of all specimens fabricated by 3D printing were analyzed, and the ultimate tensile strength, tensile modulus, and tensile strain values derived from the stress–strain curves are summarized in Table 3. These values were found to be consistent with those reported in the manufacturers' data sheets, as summarized in Table 1. The ultimate tensile strength (UTS) represents the maximum stress sustained before fracture and was selected as the comparative criterion in this study, rather than yield strength. This choice was made because sudden stress drops observed in multi-material specimens correspond to localized yielding in one of the constituent polymers, while the other remains in the elastic region, making yield strength comparison scientifically unreliable. The tensile modulus was determined from the initial linear portion of the stress–strain curve, reflecting material stiffness. The tensile strain corresponds to elongation at break for ductile materials and to the stress-drop point for brittle ones [36–38].

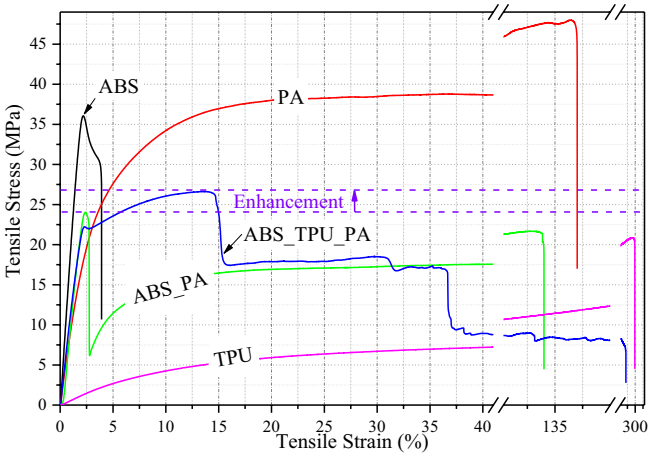

FIGURE 7 | Representative stress–strain curves of specimens: ABS, PA, TPU, ABS_PA, and ABS_TPU_PA.

In this study, poor interfacial adhesion was observed in the ABS_PA specimens fabricated via multi-material 3D printing. The data presented in Table 3 supports this observation. Specifically, the UTS values of the ABS_PA multi-material specimens were approximately 33% lower than those of ABS and about 49% lower than those of PA, indicating significant interfacial weakness. This reduction can be attributed to the lack of chemical compatibility between ABS and PA, as well as to differences in their mechanical behavior and deformation characteristics, which promote interfacial separation under applied stress [39].

To improve the interface compatibility between ABS and PA, PLA was introduced as a compatibilizing interlayer, and its effect is evaluated through representative stress–strain curves presented in Figure 3. The results indicate that the ABS_PLA_PA specimen exhibits higher UTS and tensile modulus compared to the ABS_PA, reflecting improved interfacial bonding due to the PLA layer. Improved compatibility is provided by the

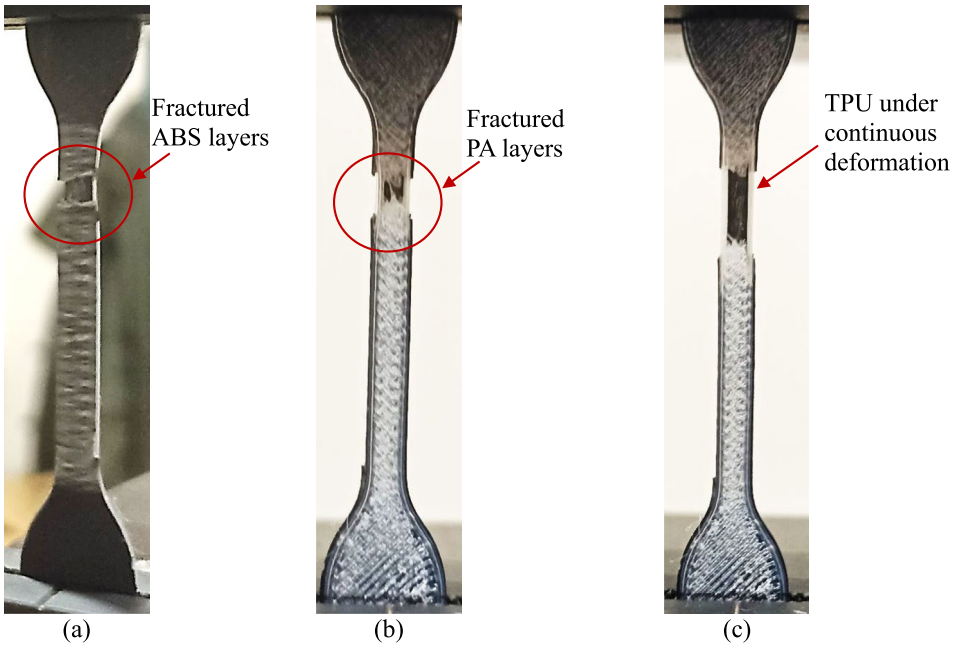

FIGURE 8 | Representative images showing yield and fracture points: (a) fracture of ABS, (b) fracture of PA (excluding wall lines), and (c) yielding of TPU and PA wall lines prior to fracture.

15480585, 0, Downloaded from https://4spepublications.onlinelibrary.wiley.com/doi/10.1002/vnl.70051 by Sinan YILMAZ - Kocaeli Üniversitesi , Wiley Online Library on [06/12/2025]. See the Terms and Conditions (https://onlinelibrary.wiley.com/terms-and-conditions) on Wiley Online Library for rules of use; OA articles are governed by the applicable Creative Commons License

PLA interlayer. Enhanced compatibility between the materials under tensile loading also resulted in smoother strain behavior without abrupt stress drops.

In this laminar composite configuration, two distinct interfaces exist: One between ABS and PLA, and the other between PLA and PA. These interfaces exhibit different bonding behaviors, which should be assessed separately [40]. Incorporation of the PLA interlayer increased the ultimate tensile strength (UTS) by approximately 32% and the tensile modulus by about 23% compared with ABS_PA, indicating stronger adhesion at the ABS/PLA interface. However, the improved interfacial strength was accompanied by a noticeable reduction in tensile strain, suggesting a trade-off between stiffness and ductility.

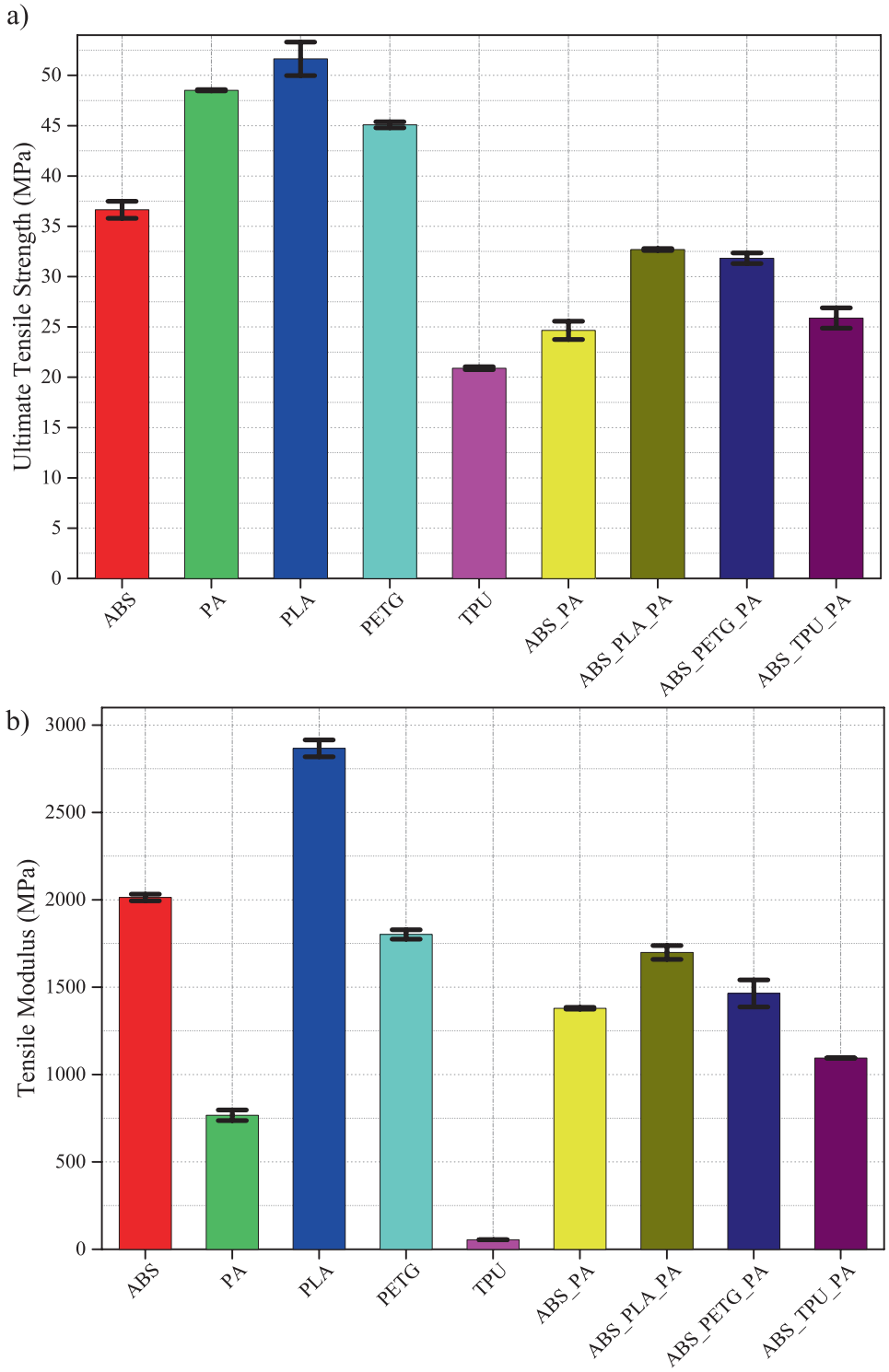

FIGURE 9 | Comparative bar charts of (a) ultimate tensile strength, (b) Young's (tensile) modulus, and (c) tensile strain for all material configurations.

15480585, 0, Downloaded from https://4spepublications.onlinelibrary.wiley.com/doi/10.1002/vnl.70051 by Sinan YILMAZ - Kocaeli Universitesi , Wiley Online Library on [06/12/2025]. See the Terms and Conditions (https://onlinelibrary.wiley.com/terms-and-conditions) on Wiley Online Library for rules of use; OA articles are governed by the applicable Creative Commons License

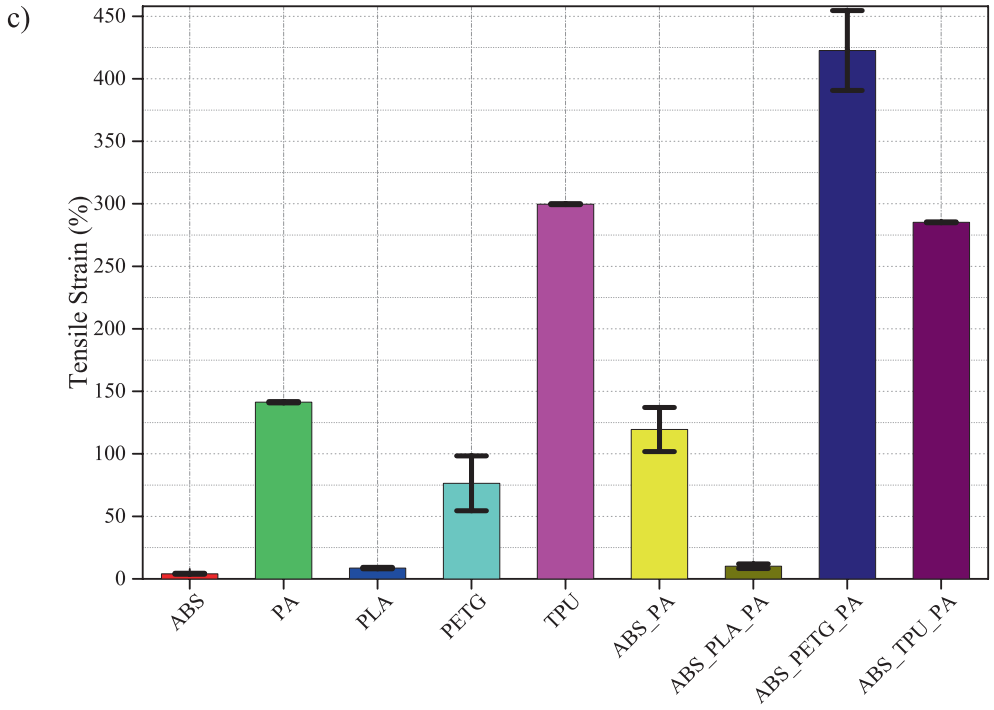

FIGURE 9 | (Continued)

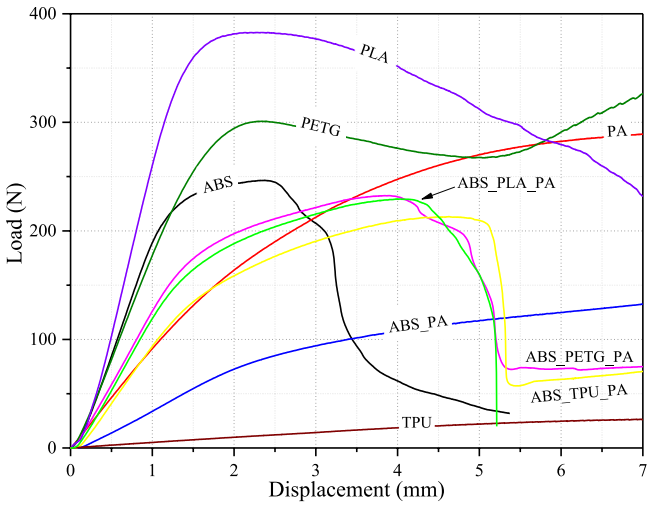

FIGURE 10 | Representative load–displacement curves obtained from ILSS tests.

The photographs in Figure 4 illustrate the deformation behavior of the multilayer specimens during tensile loading. In the reference ABS_PA structure, the two polymers show almost no adhesion, as also reflected in the stress–strain curve in Figure 3, where an abrupt load drop occurs after the fracture of the ABS layer, followed by the PA layer continuing to deform up to about 130% strain before failure. When PLA interlayers are introduced between ABS and PA, the deformation pattern changes. Because PLA is stiffer than both polymers, it increases the overall modulus of the composite. During loading, the PLA layers deform together with ABS and fail at an earlier stage, as evidenced by the exposure of the light-colored PA layer once the ABS_PLA sublayers rupture. Although PLA fractures earlier, it provides stronger interfacial interaction with ABS and improved adhesion with PA under optimized process conditions [41], which, as supported by the data in Table 3, results in an increase in the overall UTS of the multilayer structure.

The interfacial compatibility between ABS and PA was further examined by investigating the use of a PETG compatibility layer, based on tensile test results. The representative tensile stress–strain curves of PETG and ABS_PETG_PA were also illustrated in Figure 5 alongside the common curves. PETG exhibited a tensile strength value close to that of PA but slightly lower, whereas its tensile modulus was more comparable to that of ABS. In terms of elongation, PETG showed intermediate ductility between ABS and PA. This balanced mechanical response suggests that PETG provides a favorable combination of stiffness and deformability, facilitating improved interfacial adhesion between the two polymers.

When PETG was used as an interfacial compatibilizer, the ultimate tensile strength, tensile modulus, and tensile strain values all increased by approximately 29%, 6%, and 253%, respectively, compared to those of ABS_PA (excluding standard deviations). These initial findings indicate that PETG has potential as an effective interfacial layer between ABS and PA.

When the two interfaces in the structure are examined separately, the following observations can be made. As shown in the in situ photographs during the tensile test (Figure 6a,b), fracture initiates in the ABS layer; however, the PETG interlayer remains well adhered to the fractured ABS surfaces and forms filament-like bridges (strands) that continue to transfer load across the crack. At the PETG-PA interface (Figure 6c), although continuous adhesion is not fully achieved, the two

15480585, 0, Downloaded from https://4spepublications.onlinelibrary.wiley.com/doi/10.1002/vnl.70051 by Sinan YILMAZ - Kocaeli Universitesi , Wiley Online Library on [06/12/2025]. See the Terms and Conditions (https://onlinelibrary.wiley.com/terms-and-conditions) on Wiley Online Library for rules of use; OA articles are governed by the applicable Creative Commons License

materials deform together until final failure, indicating partial mechanical interlocking and load sharing between the layers.

The final part of the tensile analysis evaluated the effect of TPU as a compatibilizing interlayer, as shown in the stress–strain curves in Figure 7. As expected, TPU exhibited much lower tensile strength and modulus than ABS and PA, but its elongation at break reached approximately 300%, indicating a highly ductile nature. When TPU was incorporated between ABS and PA, the ultimate tensile strength increased by about 5%, whereas the tensile modulus decreased by around 21% compared with ABS-PA, reflecting the intrinsically soft and elastic behavior of TPU. In contrast, the tensile strain increased significantly (by roughly 140%), confirming the strain-absorbing and stress-dispersing function of TPU at the interface.

Real-time images captured during the tensile tests were used to monitor the deformation and fracture sequence of the multilayer specimens. As shown in Figure 8, fracture initiated in the ABS layer at an early stage (around 15% overall strain), while the TPU and PA layers continued to elongate (Figure 8a). The TPU layer acted as a stress-relieving interface, allowing the PA layer to carry the load and deform further until rupture at approximately 35% strain (Figure 8b). As illustrated in Figure 8c, the TPU interlayer and the unbroken PA wall lines sustained the applied load until the complete failure of both materials.

To facilitate a comprehensive comparison of the mechanical performance across all material configurations, the ultimate tensile strength, tensile modulus, and tensile strain values summarized in Table 3 were visualized in Figure 9. This comparative chart enables clearer interpretation of trends and differences among the compatibilizer designs. By presenting these data at the end of the tensile analysis, the key findings are effectively synthesized and contextualized before moving to the subsequent discussion of interfacial bonding (ILSS) behavior.

3.2 | ILSS Test Results

ILSS tests were performed to evaluate the interfacial adhesion between different layers in the multilayered structures. Unlike uniaxial tensile tests, the ILSS test provides a more direct assessment of shear-induced delamination, which is critical in layered composites where failure often initiates at the interfaces. In these tests, specimens were subjected to three-point bending to generate significant shear stresses along the interfaces without causing complete fracture. The resulting force–displacement data were used to determine the ILSS values for all material combinations, calculated according to Equation (1), allowing for a comparative assessment of interfacial bonding performance. The calculated values are presented in table 4 as averages with their corresponding standard deviations [42].

The load–displacement curves obtained from the ILSS tests for all specimen types are presented in Figure 10. These curves were used to calculate the ILSS values, which are comparatively illustrated in Figure 11. The corresponding deformation and failure behaviors captured during ILSS testing are shown in Figure 12 to provide a visual correlation with the mechanical responses.

Examining the ILSS values in Figure 11 (excluding standard deviations) shows that, among the single-material specimens, PLA has the highest value, followed by PA and PETG, then ABS, with TPU the lowest. The representative load–displacement curves in Figure 10 are consistent with this trend. A closer examination of the load–displacement curves in Figure 10 reveals that ABS fails after a relatively small deformation, characterized by a sharp load drop—an indication of its brittle behavior (Figure 12a). On the other hand, the PA sample responded to the applied force with a relatively low and steady slope, consistent with its elastic behavior (Figure 12b).

The ABS_PA multi-material specimen, composed of 10 layers of ABS followed by 10 layers of PA, displays a dual-slope profile in

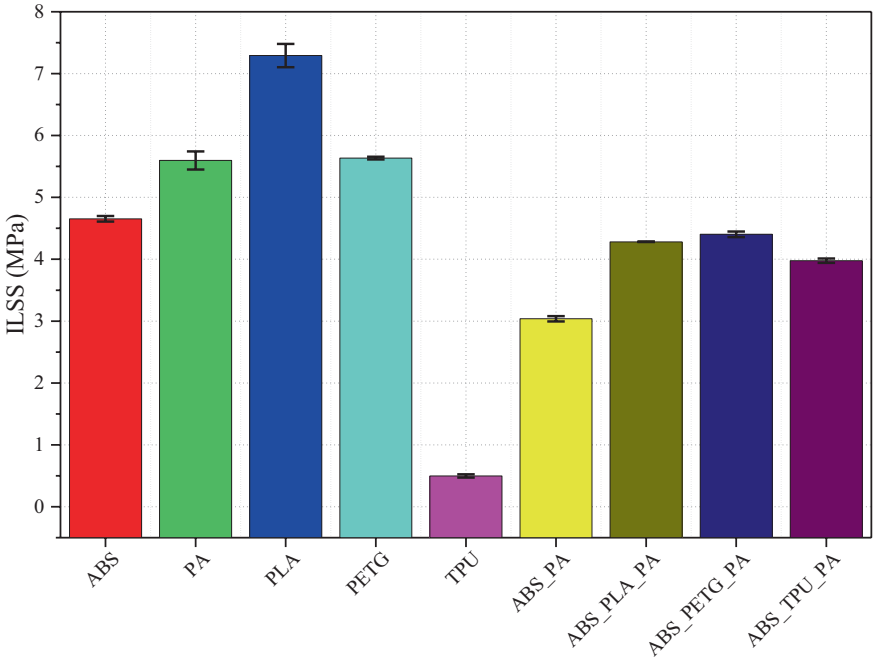

FIGURE 11 | Comparison of ILSS values for different material configurations based on ILSS test results.

15480585, 0, Downloaded from https://4spepublications.onlinelibrary.wiley.com/doi/10.1002/vnl.70051 by Sinan YILMAZ - Kocaeli Üniversitesi , Wiley Online Library on [06/12/2025]. See the Terms and Conditions (https://onlinelibrary.wiley.com/terms-and-conditions) on Wiley Online Library for rules of use; OA articles are governed by the applicable Creative Commons License

its force-displacement curve (Figure 10). The initial region corresponds to the thinner ABS section and exhibits a steep slope, albeit lower than that of the standard ABS sample. This reduction is primarily due to the thinner ABS section in the multilayer configuration, which lowers the ILSS because of its reduced effective load-bearing area at the interface. Following the fracture of the ABS segment, PA takes over the load with a lower slope. The sequential load-bearing transition and overall low ILSS indicate weak interfacial adhesion between ABS and PA, leading to early delamination or crack propagation along the interface, as illustrated in Figure 12f.

Specimens incorporating a compatibilizing layer (PLA, PETG, or TPU) between ABS and PA exhibited significantly enhanced ILSS performance. As shown in Figure 11, the ILSS trend was observed as ABS_PETG_PA > ABS_PLA_PA > ABS_TPU_PA. While all compatibilizers improved interfacial adhesion, the mechanisms behind their effectiveness differ.

ABS_PLA_PA specimen benefits from PLA's high compatibility with ABS and moderate interaction with PA, resulting in increased initial stiffness and improved interfacial continuity, as seen in Figure 12g. In the ABS_PETG_PA specimen, PETG

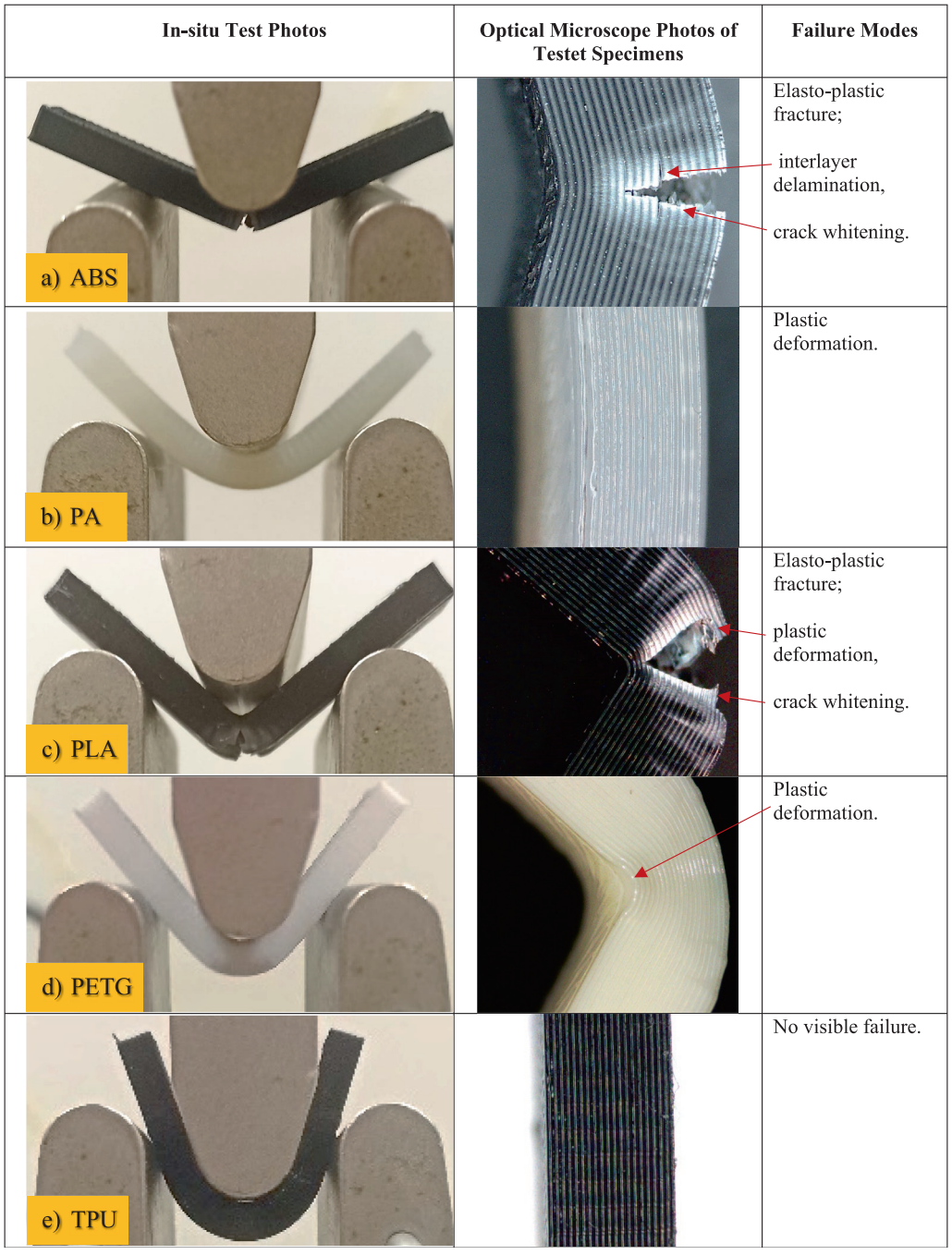

FIGURE 12 | Summary of failure behaviors observed during interlaminar shear strength (ILSS) tests. Images are representative of typical fracture modes for each configuration.

15480585, 0, Downloaded from https://4spepublications.onlinelibrary.wiley.com/doi/10.1002/vnl.70051 by Sinan YILMAZ - Kocaeli Universitesi , Wiley Online Library on [06/12/2025]. See the Terms and Conditions (https://onlinelibrary.wiley.com/terms-and-conditions) on Wiley Online Library for rules of use; OA articles are governed by the applicable Creative Commons License

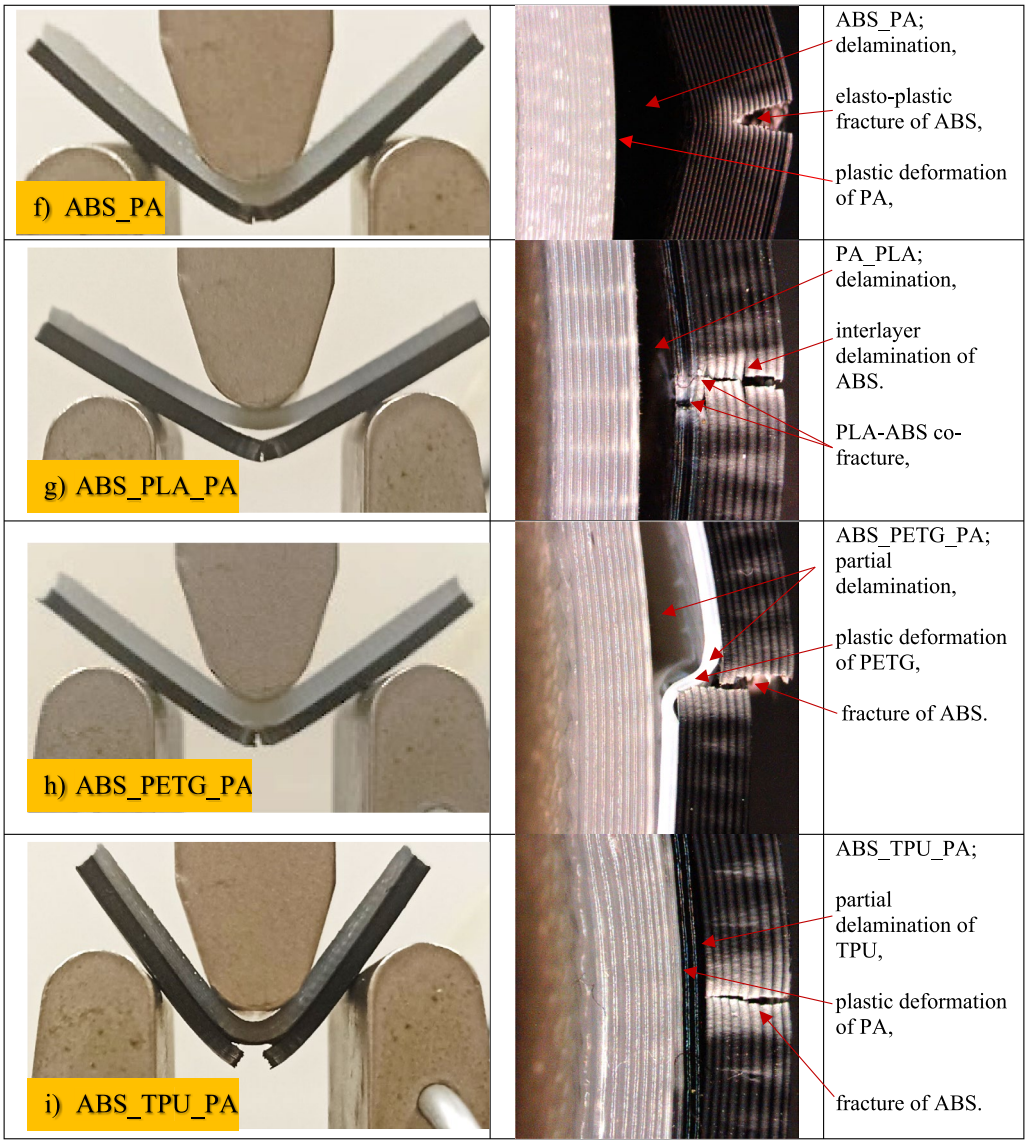

FIGURE 12 | (Continued)

shows strong adhesion to both ABS and PA, which enhances interfacial strength (see Table 4) and results in a stiffer and more cohesive response. Figure 12h illustrates the PETG layer undergoing plastic deformation under load, contributing to a jagged but robust force-displacement profile.

On the other hand, TPU provides a particularly notable case. Although TPU exhibits inherently lower ILSS and modulus compared to ABS and PA, its inclusion as a compatibilizer layer significantly enhances the overall interlaminar bonding behavior of the multilayer composite. This improvement can be attributed to TPU's elastomeric nature, which acts as a stress-relief interlayer, mitigating stress concentration at the ABS/PA interface. By accommodating differential strains and enabling gradual load transfer between the stiff ABS and PA layers, TPU effectively delays crack initiation and propagation under bending loads. In addition to this stress-buffering effect, TPU's lower viscosity during the printing process allows it to flow more effectively onto adjacent polymer surfaces, filling in surface asperities created by the layer-by-layer deposition process (related to the low viscosity of the material, see MFI for TPU in Table 4) [43]. This results in a form of mechanical interlocking that reinforces interfacial integrity. This mechanism is supported by the extended displacement observed in Figure 12i, indicating more distributed deformation and delayed failure [44].

The interfacial adhesion trends observed in this study can be attributed to the combined influence of chemical compatibility and thermal interaction among the polymers. Although ABS and PA inherently exhibit weak interfacial bonding due to their distinct chemical structures and thermal behavior, the introduction of compatibilizing interlayers significantly improved adhesion.

PLA enhanced interfacial performance through its partial affinity with both polymers, as the ester groups in PLA can interact with the amide groups of PA, whereas its backbone promotes good adhesion with ABS, thereby enhancing stiffness and interfacial continuity [45–47]. PETG, owing to its amorphous nature and intermediate glass transition temperature (~80°C), acted as a thermal bridge between ABS and PA, mitigating residual

15480585, 0, Downloaded from https://4spepublications.onlinelibrary.wiley.com/doi/10.1002/vnl.70051 by Sinan YILMAZ - Kocaeli Universitesi , Wiley Online Library on [06/12/2025]. See the Terms and Conditions (https://onlinelibrary.wiley.com/terms-and-conditions) on Wiley Online Library for rules of use; OA articles are governed by the applicable Creative Commons License

TABLE 4 | ILSS results of all specimens.

	ABS	PA	PLA	PETG	TPU	ABS_PA	ABS_PLA_PA	ABS_PETG_PA	ABS_TPU_PA
ILSS (MPa)	4.7 ± 0.1	5.6 ± 0.15	7.3 ± 0.19	5.6 ± 0.02	0.5 ± 0.03	3.0 ± 0.04	4.3 ± 0.01	4.4 ± 0.04	4.0 ± 0.04

stresses and enhancing interfacial strength [48, 49]. TPU, with its elastomeric and polar character, further improved adhesion by enabling hydrogen bonding between its urethane/urea groups and the amide groups in PA, whereas also serving as a compliant interlayer that relieved thermal and mechanical stresses during loading [50, 51].

These findings collectively indicate that the synergistic optimization of chemical affinity and thermal compatibility is key to enhancing bonding strength in multi-material FFF structures. Despite their distinct mechanical and rheological characteristics, all three compatibilizing layers contributed to improved load transfer and delayed interfacial failure, reinforcing the importance of tailored interlayer design in multi-material 3D-printed structures.

4 | Conclusions

The present study demonstrates that integrating compatibilizing interlayers between chemically incompatible thermoplastics, such as ABS and PA, can substantially enhance interfacial performance in multi-material fused filament fabrication. All tested compatibilizers (PLA, PETG, and TPU) improved both tensile and interlaminar shear properties compared with direct ABS/PA stacking.

The most significant tensile enhancement was achieved with PLA, resulting in a 32% increase in ultimate tensile strength. In contrast, PETG provided the best balance between strength and ductility. Although TPU possesses lower intrinsic stiffness, its viscoelastic nature contributed to approximately a 33% improvement in interlaminar shear strength, attributed to its stress-dispersing behavior at the interface.

These findings highlight that the mechanical integrity of multi-material 3D-printed structures can be tuned through the judicious selection of interlayer materials, enabling the fabrication of hybrid polymer components with tailored stiffness and flexibility. The proposed approach offers a straightforward and scalable route to improve adhesion between dissimilar polymers without requiring surface treatment or chemical compatibilizers, making it relevant for industrial applications such as lightweight automotive or consumer components.

Future research should extend this concept to gradient or functionally graded interfaces, in situ process monitoring, and recycled or bio-based filament systems toward more sustainable and high-performance additive manufacturing.

Author Contributions

Okan Gul: methodology, investigation, validation, data curation, project administration, visualization, funding acquisition. **Sinan Yilmaz:** conceptualization, methodology, software, validation, investigation, visualization, resources, writing – review and editing, data curation, supervision, formal analysis. **Onur Coban:** supervision, writing – original draft, writing – review and editing, visualization, formal analysis.

Funding

This work was supported by the Scientific Research Projects Coordination Unit of Kocaeli University (FHD-2024-3631).

15480585, 0, Downloaded from https://4spepublications.onlinelibrary.wiley.com/doi/10.1002/vnl.70051 by Sinan YILMAZ - Kocaeli Universitesi , Wiley Online Library on [06/12/2025]. See the Terms and Conditions (https://onlinelibrary.wiley.com/terms-and-conditions) on Wiley Online Library for rules of use; OA articles are governed by the applicable Creative Commons License

Conflicts of Interest

The authors declare no conflicts of interest.

Data Availability Statement

Research data are not shared.

References

1. K. V. Wong and A. Hernandez, "A Review of Additive Manufacturing," *ISRN Mechanical Engineering* 2012 (2012): 1–10, https://doi.org/10.5402/2012/208760.

2. S. Kumar, R. Singh, T. P. Singh, and A. Batish, "Fused Filament Fabrication: A Comprehensive Review," *Journal of Thermoplastic Composite Materials* 36, no. 2 (2020): 1–814, https://doi.org/10.1177/0892705720970629.

3. X. Wang, M. Jiang, Z. Zhou, J. Gou, and D. Hui, "3D Printing of Polymer Matrix Composites: A Review and Prospective," *Composites Part B: Engineering* 110 (2017): 442–458, https://doi.org/10.1016/j.compositesb.2016.11.034.

4. R. S. Odera and C. I. Idumah, "Novel Advancements in Additive Manufacturing of PLA: A Review," *Polymer Engineering and Science* 63 (2023): 1–20, https://doi.org/10.1002/pen.26450.

5. A. Pirondi, F. Moroni, and D. Ambrosini, "Effect of Infill Ratio on Fracture Toughness of Fused Filament Fabrication (FFF) Polymeric Adhesive Joints," *Journal of Adhesion* 98 (2022): 606–636, https://doi.org/10.1080/00218464.2021.1986019.

6. J. Kechagias and S. Zaoutsos, "Effects of 3D-Printing Processing Parameters on FFF Parts' Porosity: Outlook and Trends," *Materials and Manufacturing Processes* 39 (2024): 804–814, https://doi.org/10.1080/10426914.2024.2304843.

7. S. Yilmaz, "Comparative Investigation of Mechanical, Tribological and Thermo-Mechanical Properties of Commonly Used 3D Printing Materials," *European Journal of Science and Technology* (2022): 827–831, https://doi.org/10.31590/ejosat.1040085.

8. S. Yilmaz, O. Gul, B. Eyri, N. Gamze Karsli Yilmaz, and T. Yilmaz, "Comprehensive Characterization of 3D-Printed Bamboo/Poly(Lactic Acid) Bio Composites," *Polymer Engineering and Science* 63 (2023): 2958–2972, https://doi.org/10.1002/pen.26419.

9. S. W. Ahmed, G. Hussain, K. Altaf, et al., "On the Effects of Process Parameters and Optimization of Interlaminate Bond Strength in 3D Printed ABS/CF-PLA Composite," *Polymers* 12 (2020): 2155, https://doi.org/10.3390/POLYM12092155.

10. M. Samykano, S. K. Selvamani, K. Kadirgama, W. K. Ngui, G. Kanagaraj, and K. Sudhakar, "Mechanical Property of FDM Printed ABS: Influence of Printing Parameters," *International Journal of Advanced Manufacturing Technology* 102 (2019): 2779–2796, https://doi.org/10.1007/s00170-019-03313-0.

11. S. Yilmaz, T. Yilmaz, and B. Kahraman, "Essential Work of Fracture Analysis of Short Glass Fiber and/or Calcite Reinforced ABS/PA6 Composites," *Polymer Engineering and Science* 54 (2014): 540–550, https://doi.org/10.1002/pen.23584.

12. J. Utz, A. Ferbert, N. Geis, and H. Ruckdäschel, "Mechanical Properties and Predictive Analysis of Multi-Material Polypropylene-Glass Fiber Sandwich Structures Produced by Material Extrusion," *Polymer Composites* 46 (2025): 10239–10253, https://doi.org/10.1002/pc.29617.

13. I. Khan, I. Barsoum, M. Abas, A. Al Rashid, M. Koç, and M. Tariq, "A Review of Extrusion-Based Additive Manufacturing of Multi-Materials-Based Polymeric Laminated Structures," *Composite Structures* 349 (2024): 118490, https://doi.org/10.1016/j.compstruct.2024.118490.

14. G. Pathinettampadian, M. Vellaisamy, T. Kumar Muthu Kumar, M. Agnelo Browne, and M. Kumar Subramaniyan, "Some Studies on Functional Behavior of Novel Multi-Layered Material for Integrated Structural Application," *Journal of Industrial and Engineering Chemistry* 131 (2024): 545–557, https://doi.org/10.1016/j.jiec.2023.10.059.

15. A. Fakhr Ghasemi and J. Pinto Duarte, "A Systematic Review of Innovative Advances in Multi-Material Additive Manufacturing: Implications for Architecture and Construction," *Materials* 18 (2025): 1820, https://doi.org/10.3390/ma18081820.

16. A. K. Singh and Siddhartha, "A Novel Technique for In-Situ Manufacturing of Functionally Graded Materials Based Polymer Composite Spur Gears," *Polymer Composites* 40 (2019): 523–535, https://doi.org/10.1002/pc.24682.

17. Y. Zhang, C. Purssell, K. Mao, and S. Leigh, "A Physical Investigation of Wear and Thermal Characteristics of 3D Printed Nylon Spur Gears," *Tribology International* 141 (2020): 105953, https://doi.org/10.1016/j.triboint.2019.105953.

18. R. Boros, A. Tatyana, Á. Golcs, O. H. Krafcsik, and J. G. Kovács, "Plasma Treatment to Improve the Adhesion Between ABS and PA6 in Hybrid Structures Produced by Injection Overmolding," *Polymer Testing* 106 (2022): 107446, https://doi.org/10.1016/j.polymertesting.2021.107446.

19. J. D. Kechagias, N. A. Fountas, I. Papantoniou, and N. M. Vaxevanidis, "Interlaminar Bonding Assessment in Vertical-Oriented Filament Material Extrusion Bending Specimens," *International Journal of Advanced Manufacturing Technology* 136 (2025): 4977–4989, https://doi.org/10.1007/s00170-025-15124-7.

20. E. A. Papon, A. Haque, and S. K. Spear, "Effects of Functionalization and Annealing in Enhancing the Interfacial Bonding and Mechanical Properties of 3D Printed Fiber-Reinforced Composites," *Materials Today Communications* 25 (2020): 101365, https://doi.org/10.1016/J.MTCOMM.2020.101365.

21. M. A. E. Omer, I. A. Shaban, A. H. Mourad, and H. Hegab, "Advances in Interlayer Bonding in Fused Deposition Modelling: A Comprehensive Review," *Virtual and Physical Prototyping* 20 (2025): 2522951, https://doi.org/10.1080/17452759.2025.2522951.

22. S. Wickramasinghe, T. Do, and P. Tran, "FDM-Based 3D Printing of Polymer and Associated Composite: A Review on Mechanical Properties, Defects and Treatments," *Polymers* 12 (2020): 1–42, https://doi.org/10.3390/polym12071529.

23. M. E. Spreeman, H. A. Stretz, and M. D. Dadmun, "Role of Compatibilizer in 3D Printing of Polymer Blends," *Additive Manufacturing* 27 (2019): 267–277, https://doi.org/10.1016/j.addma.2019.03.009.

24. A. Bandyopadhyay and B. Heer, "Additive Manufacturing of Multi-Material Structures," *Materials Science & Engineering R: Reports* 129 (2018): 1–16, https://doi.org/10.1016/j.mser.2018.04.001.

25. S. Hasanov, S. Alkunte, M. Rajeshirke, et al., "Review on Additive Manufacturing of Multi-Material Parts: Progress and Challenges," *Journal of Manufacturing and Materials Processing* 6 (2022): 4, https://doi.org/10.3390/jmmp6010004.

26. S. P. Zaoutsos and J. D. Kechagias, "Optimizing Bonding Conditions Between Multilayer FFF Material Extrusion," *Materials and Manufacturing Processes* 40 (2025): 499–506, https://doi.org/10.1080/10426914.2024.2437753.

27. O. Gul, S. Yilmaz, and T. Yilmaz, "Effect of CBC and G-POSS on Tribological Behaviour of Polyamide 6 and Short Glass Fiber Reinforced Polyamide 6 Composites," *Acta Physica Polonica A* 127 (2015): 1121, https://doi.org/10.12693/APhysPolA.127.1121.

28. F. Baldi, F. Bignotti, G. Tieghi, and T. Riccò, "Rubber Toughening of Polyamide 6/Organoclay Nanocomposites Obtained by Melt Blending," *Journal of Applied Polymer Science* 99 (2006): 3406–3416, https://doi.org/10.1002/app.22955.

29. R. A. Kudva, H. Keskkula, and D. R. Paul, "Properties of Compatibilized Nylon 6/ABS Blends: Part I. Effect of ABS Type," *Polymer* 41 (2000): 225–237, https://doi.org/10.1016/S0032-3861(99)00105-6.

15480585, 0, Downloaded from https://4spepublications.onlinelibrary.wiley.com/doi/10.1002/vnl.70051 by Sinan YILMAZ - Kocaeli Üniversitesi , Wiley Online Library on [06/12/2025]. See the Terms and Conditions (https://onlinelibrary.wiley.com/terms-and-conditions) on Wiley Online Library for rules of use; OA articles are governed by the applicable Creative Commons License

30. A. C. Abbott, G. P. Tandon, R. L. Bradford, H. Koerner, and J. W. Baur, "Process-Structure-Property Effects on ABS Bond Strength in Fused Filament Fabrication," *Additive Manufacturing* 19 (2018): 29–38, https://doi.org/10.1016/j.addma.2017.11.002.

31. V. Mishra, C. K. Ror, S. Negi, S. Kar, and L. N. Borah, "Development of Sustainable 3D Printing Filaments Using Recycled/Virgin ABS Blends: Processing and Characterization," *Polymer Engineering and Science* 63 (2023): 1–10, https://doi.org/10.1002/pen.26330.

32. M. S. Islam and P. Prabhakar, "Interlaminar Strengthening of Multidirectional Laminates Using Polymer Additive Manufacturing," *Materials and Design* 133 (2017): 332–339, https://doi.org/10.1016/j.matdes.2017.07.038.

33. Y. Dong, T. Yu, X. j. Wang, et al., "Improved Interfacial Shear Strength in Polyphenylene Sulfide/Carbon Fiber Composites via the Carboxylic Polyphenylene Sulfide Sizing Agent," *Composites Science and Technology* 190 (2020): 108056, https://doi.org/10.1016/j.compscitech.2020.108056.

34. A. Monjon, P. Santos, S. Valvez, and P. N. B. Reis, "Hybridization Effects on Bending and Interlaminar Shear Strength of Composite Laminates," *Materials* 15 (2022): 15, https://doi.org/10.3390/ma15041302.

35. A. Kumar, K. Sharma, and A. R. Dixit, "Tensile, Flexural and Interlaminar Shear Strength of Carbon Fiber Reinforced Epoxy Composites Modified by Graphene," *Polymer Bulletin* 80 (2023): 7469–7490, https://doi.org/10.1007/s00289-022-04413-w.

36. M. Sardinha, L. Ferreira, H. Diogo, T. R. P. Ramos, L. Reis, and M. F. Vaz, "Material Extrusion of TPU: Thermal Characterization and Effects of Infill and Extrusion Temperature on Voids, Tensile Strength and Compressive Properties," *Rapid Prototyping Journal* 31 (2025): 62–81, https://doi.org/10.1108/RPJ-06-2024-0241.

37. H. M. C. C. Somarathna, S. N. Raman, D. Mohotti, A. A. Mutalib, and K. H. Badri, "Rate Dependent Tensile Behavior of Polyurethane Under Varying Strain Rates," *Construction and Building Materials* 254 (2020): 119203, https://doi.org/10.1016/j.conbuildmat.2020.119203.

38. J. Fan and A. Chen, "Studying a Flexible Polyurethane Elastomer With Improved Impact-Resistant Performance," *Polymers* 11 (2019): 11, https://doi.org/10.3390/polym11030467.

39. S. Ez-Zahraoui, Z. Kassab, E. h. Ablouh, et al., "Effect of Fly Ash and Coupling Agent on the Structural, Morphological, Thermal, and Mechanical Properties of Polyamide 6/Acrylonitrile-Butadiene-Styrene Blend," *Polymer Composites* 42 (2021): 3518–3538, https://doi.org/10.1002/pc.26076.

40. X. Shi, B. Chen, X. Tuo, Y. Gong, and J. Guo, "Study on Performance Characteristics of Fused Deposition Modeling 3D-Printed Composites by Blending and Lamination," *Journal of Applied Polymer Science* 138 (2021): 32495, https://doi.org/10.1002/app.49926.

41. M. F. Rabbi and V. Chalivendra, "Improvement in Interfacial Fracture Toughness of Multi-Material Additively Manufactured Composites Through Thermal Annealing," *Forces in Mechanics* 5 (2021): 100051, https://doi.org/10.1016/j.finmec.2021.100051.

42. Ö. Özbek, M. Bulut, A. Erkliğ, and Ö. Y. Bozkurt, "Interlaminar Shear Strength and Failure Analysis of Composite Laminates With Double and Triple Hybrid Configurations," *Engineering Structures* 265 (2022): 114498, https://doi.org/10.1016/j.engstruct.2022.114498.

43. S. Yilmaz, O. Gul, B. Eyri, N. G. Karsli, and T. Yilmaz, "Analyzing the Influence of Multimaterial 3D Printing and Postprocessing on Mechanical and Tribological Characteristics," *Macromolecular Materials and Engineering* 309 (2024): 2300428, https://doi.org/10.1002/mame.202300428.

44. M. Y. Khalid, Z. U. Arif, A. Al Rashid, et al., "Interlaminar Shear Strength (ILSS) Characterization of Fiber Metal Laminates (FMLs) Manufactured Through VARTM Process," *Forces in Mechanics* 4 (2021): 100038, https://doi.org/10.1016/j.finmec.2021.100038.

45. M. Y. Meshchankina, Y. A. Kuznetsova, M. A. Shcherbina, and S. N. Chvalun, "Biodegradable Blends Obtained via Reactive Blending of Polylactide and Polyamide-6," *Polymer Science, Series B* 58 (2016): 214–225, https://doi.org/10.1134/S1560090416020044.

46. V. Heshmati, A. M. Zolali, and B. D. Favis, "Morphology Development in Poly (Lactic Acid)/Polyamide11 Biobased Blends: Chain Mobility and Interfacial Interactions," *Polymer* 120 (2017): 197–208, https://doi.org/10.1016/j.polymer.2017.05.056.

47. H. Kuleyin, S. Budak, Ö. B. Yasan, and R. Gümrük, "Characterization of Thermal, Chemical, Mechanical, and Fatigue Behavior of 3D Printed ABS-Based Elastomeric Blends: ABS/EVA and ABS/TPU," *Polymer Testing* 145 (2025): 108763, https://doi.org/10.1016/j.polymertesting.2025.108763.

48. B. Eyri, O. Gul, S. Yilmaz, N. G. Karsli, and T. Yilmaz, "Characterization of ABS/PETG Multi-Material Composites 3D Printed by Print-Pause-Print Method," *Polymer Engineering and Science* 65 (2025): 2353–2369, https://doi.org/10.1002/pen.27151.

49. J. Yin, C. Lu, J. Fu, Y. Huang, and Y. Zheng, "Interfacial Bonding During Multi-Material Fused Deposition Modeling (FDM) Process due to Inter-Molecular Diffusion," *Materials and Design* 150 (2018): 104–112, https://doi.org/10.1016/j.matdes.2018.04.029.

50. K. Soltanmohammadi, D. Rahmatabadi, M. Aberoumand, et al., "Effects of TPU on the Mechanical Properties, Fracture Toughness, Morphology, and Thermal Analysis of 3D-Printed ABS-TPU Blends by FDM," *Journal of Vinyl & Additive Technology* 30 (2024): 958–968, https://doi.org/10.1002/vnl.22097.

51. W. Li, J. Liu, C. Hao, K. Jiang, D. Xu, and D. Wang, "Interaction of Thermoplastic Polyurethane With Polyamide 1212 and Its Influence on the Thermal and Mechanical Properties of TPU/PA1212 Blends," *Polymer Engineering and Science* 48 (2008): 249–256, https://doi.org/10.1002/pen.20853.

Supporting Information

Additional supporting information can be found online in the Supporting Information section. **Data S1:** vnl70051-sup-0001-supinfo.zip.

15480585, 0, Downloaded from https://4spepublications.onlinelibrary.wiley.com/doi/10.1002/vnl.70051 by Sinan YILMAZ - Kocaeli Üniversitesi , Wiley Online Library on [06/12/2025]. See the Terms and Conditions (https://onlinelibrary.wiley.com/terms-and-conditions) on Wiley Online Library for rules of use; OA articles are governed by the applicable Creative Commons License